Ferroelectrically controlled electromagnetic and transport properties in VN$_2$H$_2$/Al$_2$O$_3$ van der Waals multiferroic heterostructures

Caijia Sun[1], Haoshen Ye[2], Yijie Zhu[3], Leiming Chen[1], Dongmei Bai[4,*], Jianli Wang[1,*]

[1] School of Materials and Physics, China University of Mining and Technology, Xuzhou 221116, China

[2] Key Laboratory of Quantum Materials and Devices of Ministry of Education, School of Physics, Southeast University, Nanjing 211189, China

[3] National Laboratory of Solid State Microstructures and Department of Physics, Nanjing University, 210093, Nanjing, China

* Corresponding author.

E-mail address: dmbai@cumt.edu.cn (Dongmei Bai), jlwang@cumt.edu.cn (Jianli Wang).

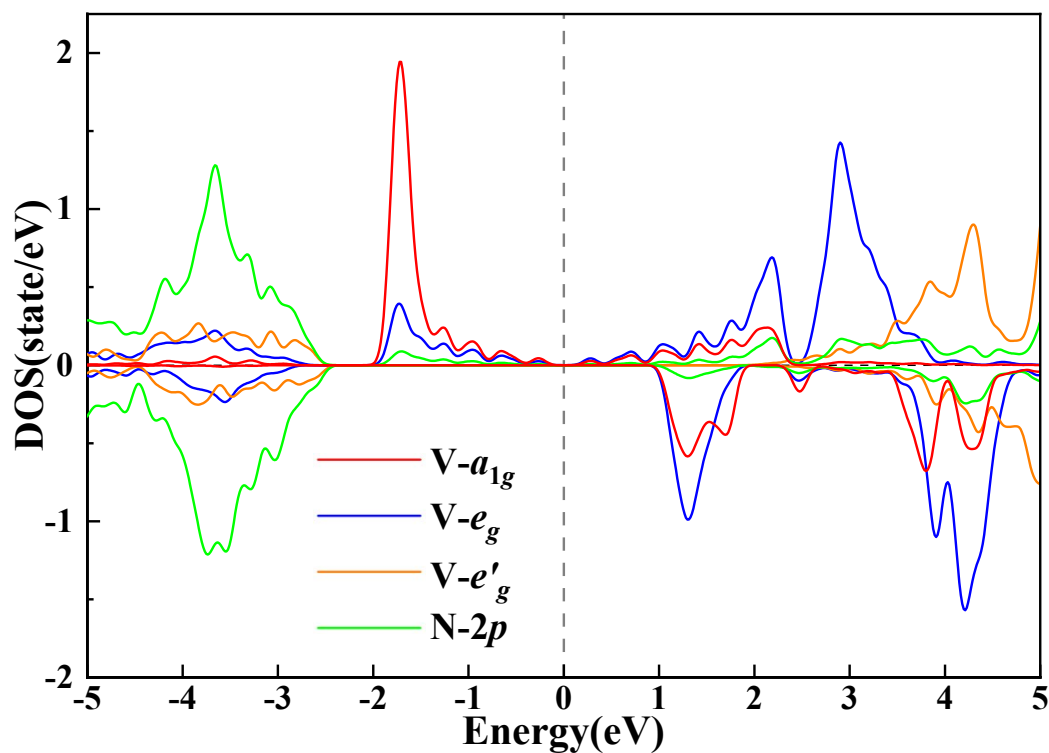**I Structure and electromagnetic properties of the VN₂H₂ monolayer and the Al₂O₃ monolayer**

Fig. S1. The orbital projected state density of the VN₂H₂ monolayer. The degenerate orbitals have been merged.
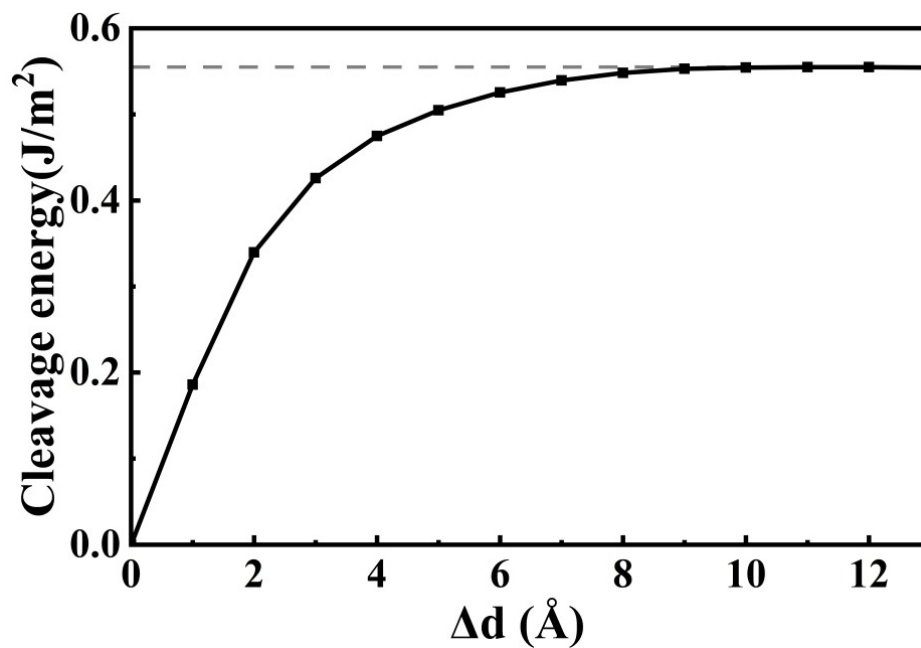

Fig. S2. The cleavage energy of the Al₂O₃ monolayer as a function of separation distance (Δd = d − d₀), where d₀ and d are the equilibrium and unequilibrium gaps.
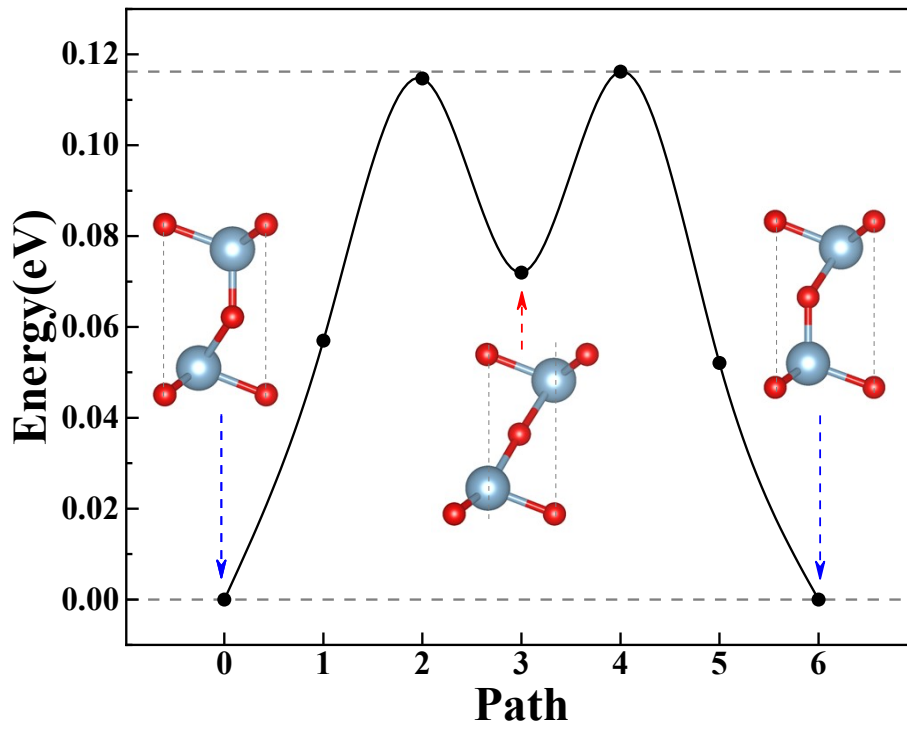
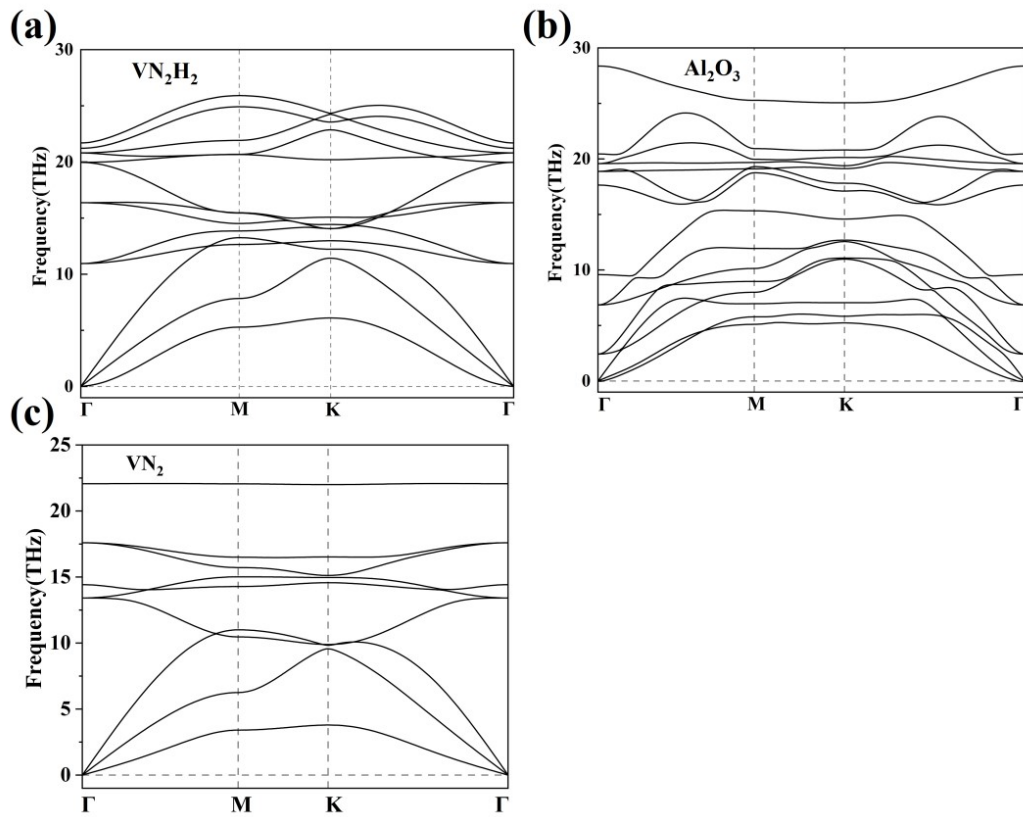**Fig. S3**. The FE transition barrier of the Al_2O_3 monolayer.

Fig. S4. The phonon spectra of the VN_2H_2 monolayer, the Al_2O_3 monolayer, and the VN_2 monolayer.
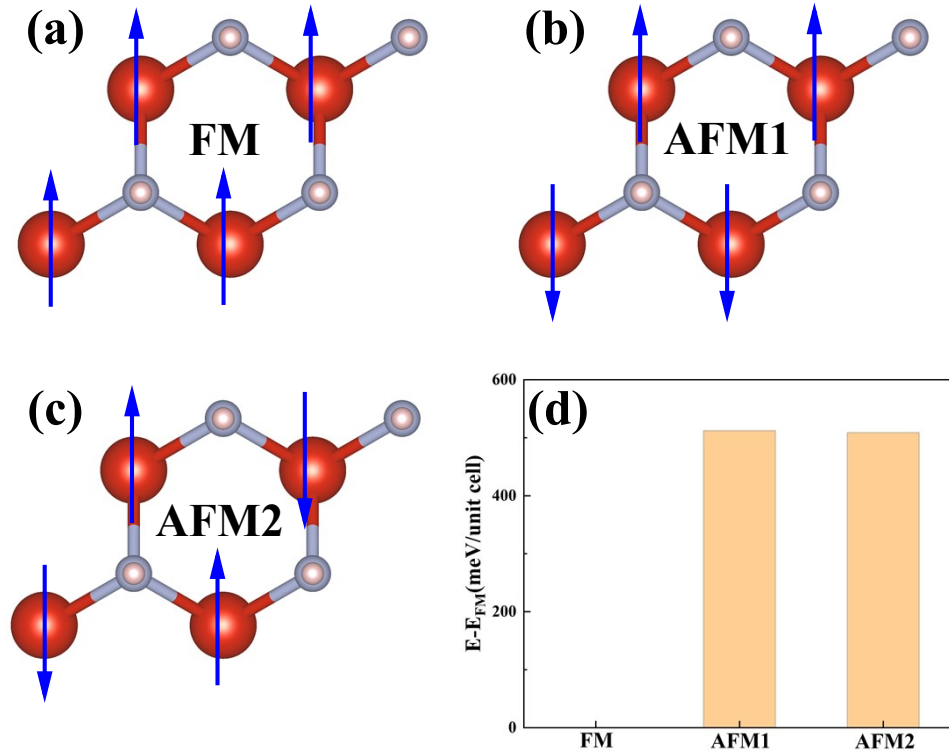
Fig. S5. The different magnetic configurations of the VN_2H_2 monolayer. (a) FM, (b) AFM1, (c) AFM2, and (d) the energy difference relative to FM in 2×2×1 supercell. The direction of the arrow represents the direction of the spin.

Table S1. The calculated lattice parameters of FM and AFM states of the VN_2H_2 monolayer, including lattice constant (a), the static energy (E_0), the length of V-N bond (L_{V-N}), the length of N-H bond (L_{N-H}), the angle of V-N-V bond (θ_{V-N-V}), the total magnetic moment (mag).

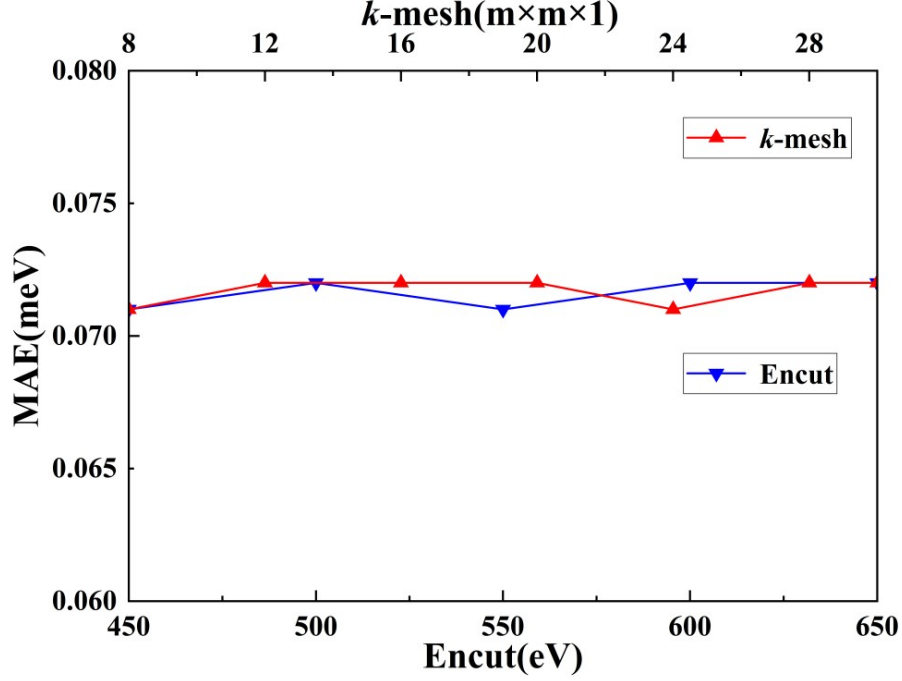|	c (Å)	E_0 (eV)	L_{V-N} (Å)	L_{N-H} (Å)	θ_{V-N-V} (°)	mag (μB)
FM	2.88	**-34.15**	2.01	1.02	91.33	1.00
AFM1	2.88	-34.02	2.00	1.02	91.51	0.00
AFM2	2.90	-34.02	2.01	1.02	91.51	0.00

Fig. S6. The magnetic anisotropy energy of the VN$_2$H$_2$ monolayer with different cutoff energy and kpoint.

II The second-order perturbation theory analysis of the magnetic anisotropy energy

The energy expression considering SOC effect is written as

$$E^{SL} = \sum_o \sum_u \frac{|\langle o|H^{SL}|u\rangle|^2}{E_o - E_u}$$

where the perturbative Hamiltonian is $H^{SL} = \lambda \vec{\sigma} \cdot \vec{L}$, and according to the expression of MAE, MAE can be represented as

$$MAE = E_{(z)} - E_{(x)} = \pm \lambda^2 \sum_{o,\,u} \frac{|\langle o|L_z|u\rangle|^2 - |\langle o|L_x|u\rangle|^2}{E_o - E_u}$$

From the orbital-resolved MAE shown in **Fig. 2** (b), the MAE of monolayer VN$_2$H$_2$ is mainly contributed by the SOC interaction of the d_{xy} orbitals and the $d_{x^2-y^2}$ orbitals of the vanadium atom. The differences of matrix elements are given in **Table S2**, and the energies of occupied and unoccupied states can be analyzed from the PDOS shown in **Fig. S7**. Since only the spin-up channel contributes to the occupied state, the expression for MAE can be written as

$$\left(d_{xy}, d_{x^2-y^2}\right) \Delta E = \lambda^2 \sum \frac{4}{E_{o^+} - E_{u^+}} + \frac{-4}{E_{o^+} - E_{u^-}} = \lambda^2\left(\frac{4}{-m} + \frac{-4}{-n}\right)$$

as shown in **Fig. S7**, m>n, the calculated MAE is positive, indicating that monolayer VN$_2$H$_2$ has

an in-plane easy magnetization axis, which is consistent with the results of DFT.

Table S2. Matrix elements differences between two magnetization directions

$$\left|\langle o^+|L_z|u^+\rangle\right|^2 - \left|\langle o^+|L_x|u^+\rangle\right|^2 \text{ and } \left|\langle o^+|L_z|u^-\rangle\right|^2 - \left|\langle o^+|L_x|u^-\rangle\right|^2$$

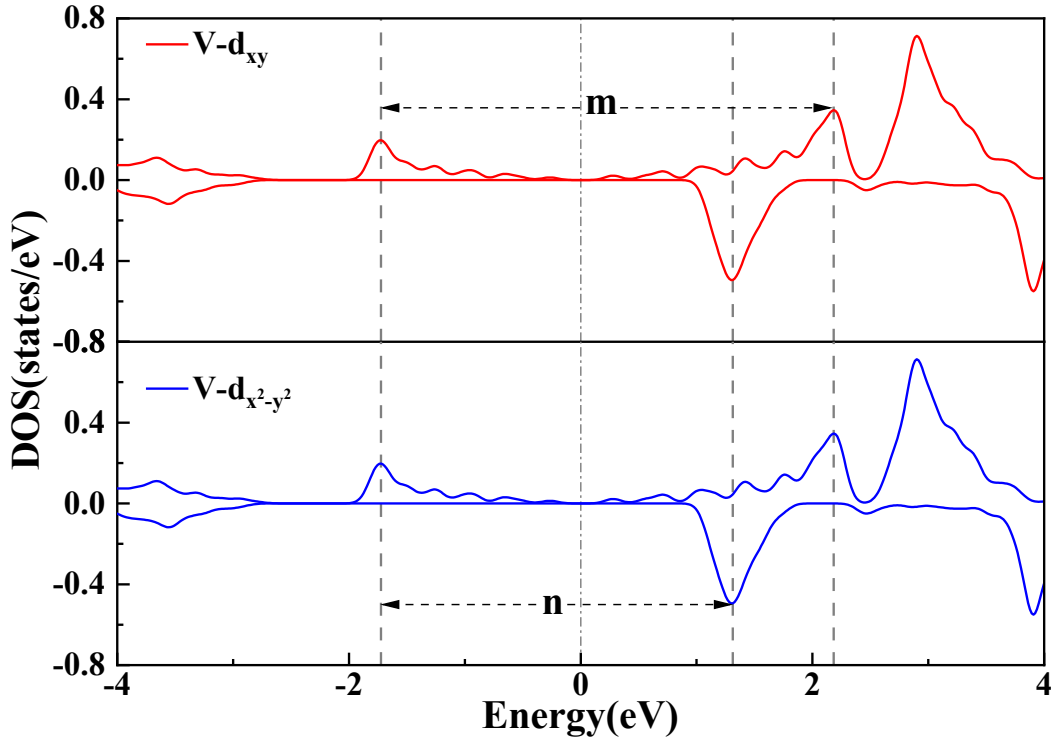| o^+	u^+					u^-				
	d_{xy}	d_{yz}	d_{z^2}	d_{xz}	$d_{x^2-y^2}$	d_{xy}	d_{yz}	d_{z^2}	d_{xz}	$d_{x^2-y^2}$
d_{xy}	0	0	0	-1	4	0	0	0	1	-4
d_{yz}	0	0	-3	1	-1	0	0	3	-1	1
d_{z^2}	0	-3	0	0	0	0	3	0	0	0
d_{xz}	-1	1	0	0	0	1	-1	0	0	0
$d_{x^2-y^2}$	4	-1	0	0	0	-4	1	0	0	0

Fig. S7. The projected densities of state of d_{xy} orbitals and $d_{x^2-y^2}$ orbitals of the VN$_2$H$_2$ monolayer.

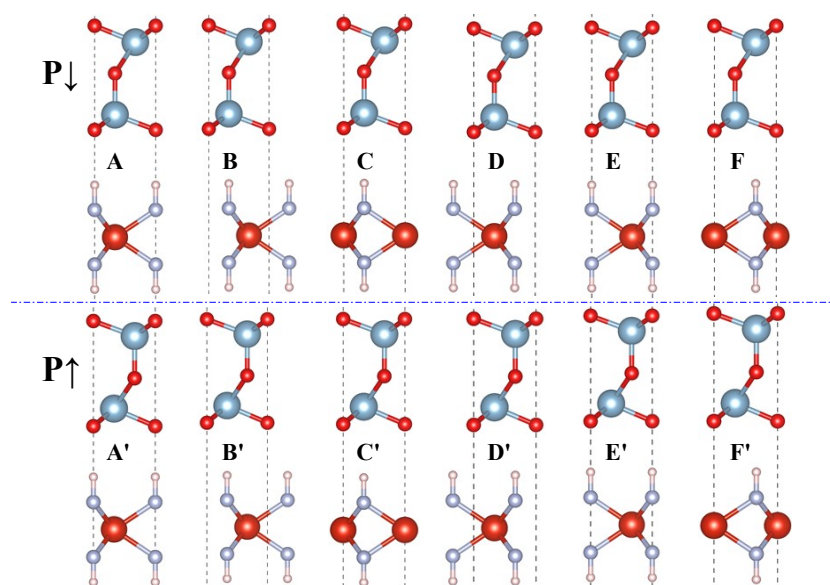**III Different stacking structural and electronic properties of the VN$_2$H$_2$/Al$_2$O$_3$ vdW**

heterostructures

Fig. S8. The stack structures of VN$_2$H$_2$/Al$_2$O$_3$ vdW heterostructures, including polarization up state and polarization down state. In the same polarization state, (A-C) is the Al$_2$O$_3$ layer fixed, the VN$_2$H$_2$ layer translated along the high symmetric point, (D-F) is the Al$_2$O$_3$ layer fixed, the VN$_2$H$_2$ layer first flipped 180° around the *z* axis, and then translated along the high symmetric point.

Table S3. Calculated parameters of VN$_2$H$_2$/Al$_2$O$_3$ vdW heterostructures with different stacking configurations, including lattice constant (a), energy difference with respect to A' configuration (ΔE), and layer spacing (d). It should be noted that all stacking configurations are FM ground state, and the energy is based on the FM state energy. Although the energy of the D' configuration is very close to that of the A' configuration, calculations with sufficient precision still show that the energy of the D' configuration is greater than that of the A' configuration, so the A' configuration is used as the ground state.

P↓	A	B	C	D	E	F
a (Å)	2.91	2.91	2.91	2.91	2.91	2.91
ΔE (meV)	102.92	119.78	119.37	102.58	102.71	102.15
d (Å)	2.28	2.28	2.28	2.16	2.28	2.16
P↑	A '	B '	C '	D '	E '	F '
a (Å)	2.91	2.91	2.91	2.91	2.91	2.91
ΔE (meV)	**0**	48.75	48.39	24.51	0.087	24.27

d (Å)	2.08	2.19	2.19	2.04	2.07	2.04
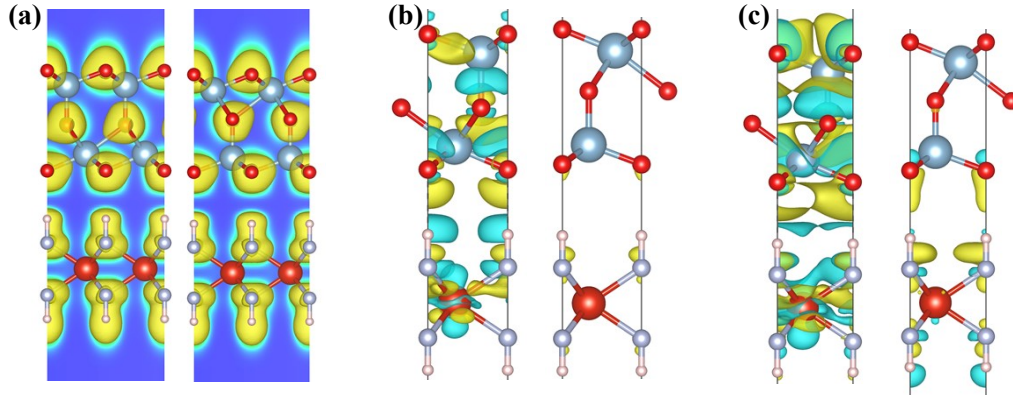
Fig. S9. (a) The electron localization function (ELF) of the VN_2H_2/Al_2O_3 (↑) state and VN_2H_2/Al_2O_3 (↓) state. The yellow region is the electron concentration region, and the blue region has no electron distribution. The charge density difference (isovalue: (b) 0.0007e·Å⁻³, (c) 0.0002 e·Å⁻³) of the VN_2H_2/Al_2O_3 vdW heterostructure. The yellow and blue distributions correspond to the charge accumulation and depletion.
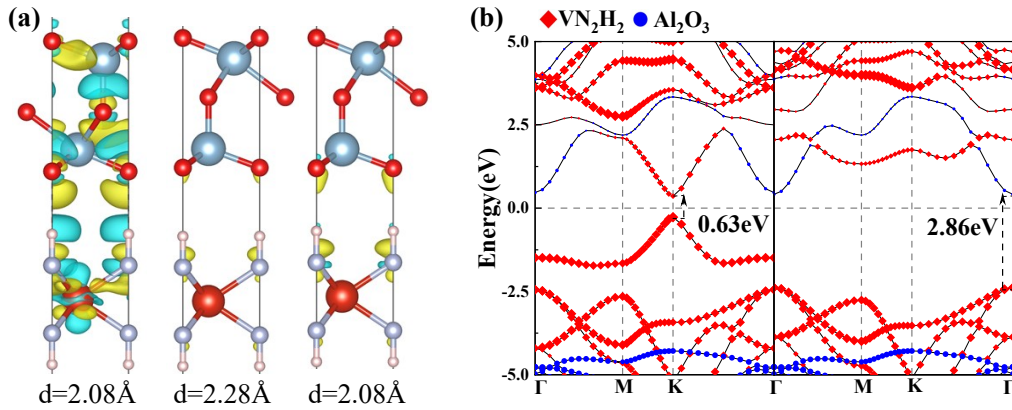

Fig. S10. (a) The charge density difference of (isovalue: 0.0007e·Å⁻³) of the VN_2H_2/Al_2O_3 vdW heterostructure with different layer spacing. (b) The band structure of VN_2H_2/Al_2O_3 (↓) with layer spacing of 2.08 Å.

IV Stability and band structures of electrostatic doping
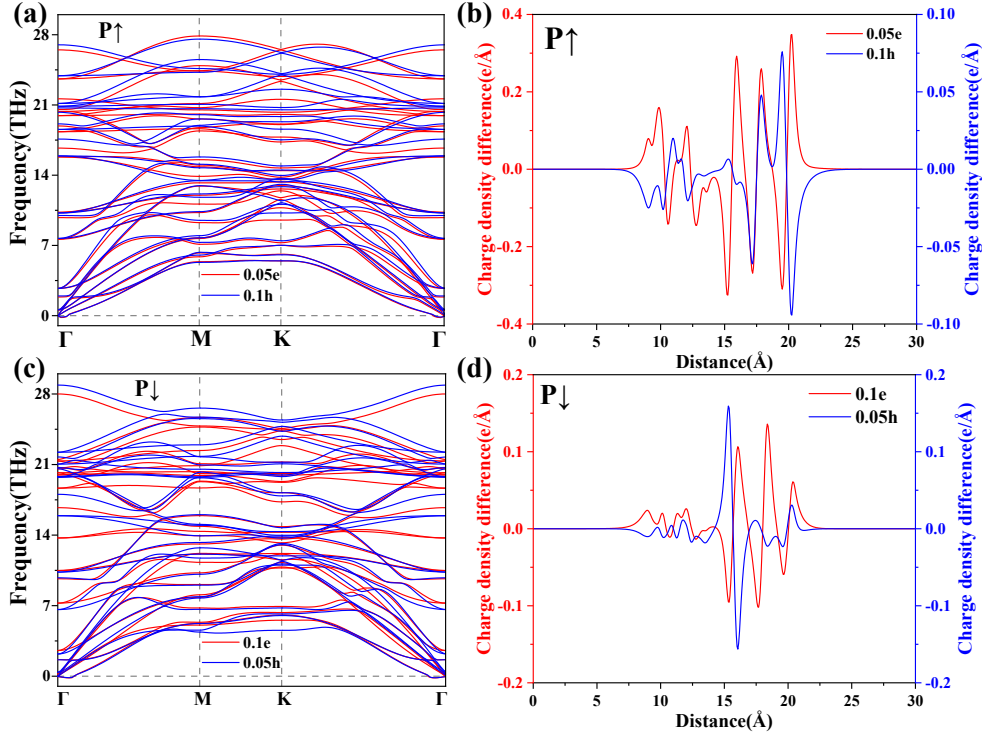
Fig. S11. (a) The phonon spectrum of the VN_2H_2/Al_2O_3 (↑) state under 0.05 *e* and 0.1 *h* per unit cell doping. (b) Charge density difference between the doped and undoped VN_2H_2/Al_2O_3 (↑) state under 0.05 *e* and 0.1 *h* per unit cell doping. (c) The phonon spectrum of the VN_2H_2/Al_2O_3 (↓) state under 0.1 *e* and 0.05 *h* per unit cell doping. (d) Charge density difference between the doped and undoped VN_2H_2/Al_2O_3 (↓) state under 0.1 *e* and 0.05 *h* per unit cell doping.
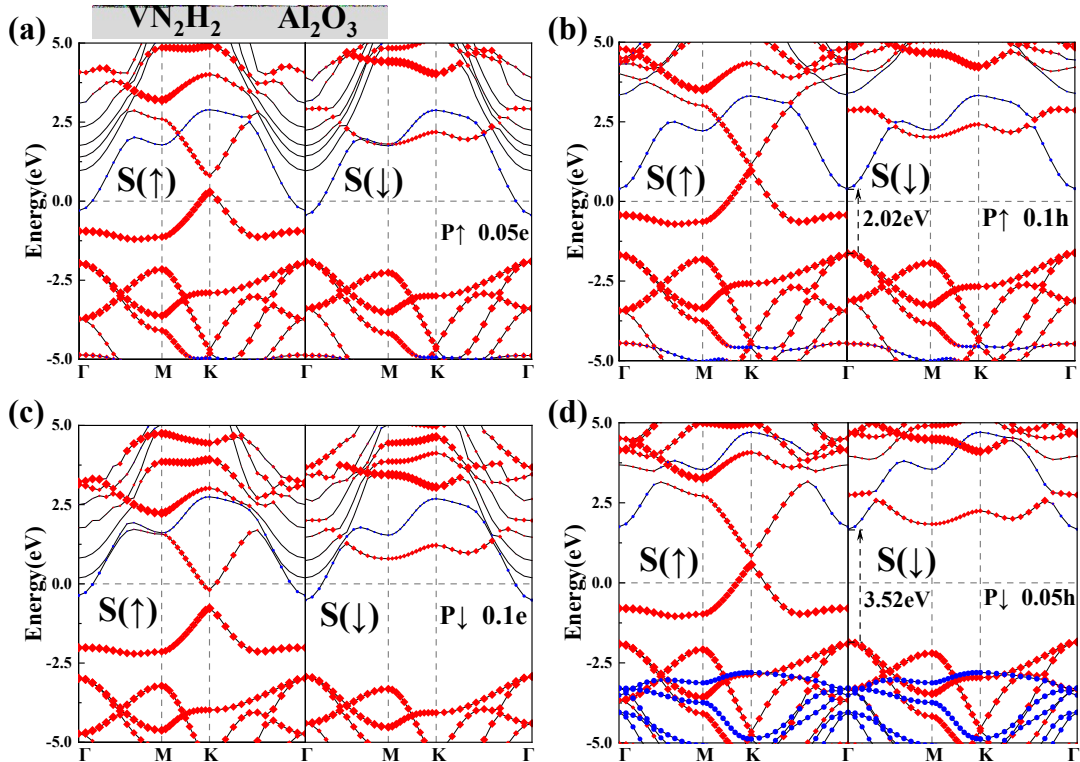
Fig. S12. The calculated band structures of the VN_2H_2/Al_2O_3 (↑) state under (a) 0.05 e and (b) 0.1 h per unit cell doping. The calculated band structures of the VN_2H_2/Al_2O_3(↓) state under (c) 0.1 e and (d) 0.05 h per unit cell doping.